Comparing the charge dynamics in MAPbBr3 and MAPbI3 using microwave photoconductance measurements

Savenije, Tom J.; Zhao, Jiashang; Caselli, Valentina M.

DOI
10.1002/9783527829026.ch9

Publication date
2023

Document Version
Accepted author manuscript

Published in
Halide Perovskite Semiconductors

Published in: Halide Perovskite Semiconductors: Structures, Characterization, Properties, and Phenomena - Editor(s):Yuanyuan Zhou, Iván Mora Seró - DOI:10.1002/9783527829026

Comparing the Charge Dynamics of $MAPbBr_3$ to $MAPbI_3$ using Microwave Photoconductance Measurements

Tom J. Savenije, Jiashang Zhao and Valentina M. Caselli*

Keywords: perovskites, charge dynamics, TRMC, transport materials, solar cells

Dr. T.J. Savenije
Jiashang Zhao
Valentina M. Caselli

Department of Chemical Engineering, Delft University of Technology, van der Maasweg 9, 2629 HZ Delft, The Netherlands

E-mail: T.J.Savenije@tudelft.nl

Perovskite-based solar cells have been rapidly developed, with record power conversion efficiencies now exceeding 25%.[1–5] In order to rationally improve the efficiency of these devices, it is important to understand and quantify the dynamics of the excess charge carriers generated on optical excitation of the metal halide perovskite (MHP) absorber layer. Furthermore, knowledge regarding the charge extraction by charge selective transport layers (CSTLs) is imperative to select proper and stable transport layers sandwiching the absorber material. In this chapter we revisit some of our earlier papers in which we have studied the charge dynamics using the Time-Resolved Microwave Conductivity (TRMC) technique. Here we will focus on two archetype MHPs *i.e.* methylammonium lead iodide ($MAPbI_3$) and methylammonium lead bromide ($MAPbBr_3$), which show, interestingly, rather different charge carrier dynamics. We will argue how these differences can be connected to variations in mobilities and trap densities. Although photoconductivity measurements do not provide specific information regarding differences in electron and hole mobility nor the type of deep trap states, by combining the MHP layer with CSTLs these matters can be disclosed.

This chapter is built up as follows: the first section comprises a short comprehensive overview regarding the electrodeless TRMC technique. Section two introduces a kinetic model to obtain

Published in: Halide Perovskite Semiconductors: Structures, Characterization, Properties, and Phenomena - Editor(s):Yuanyuan Zhou, Iván Mora Seró - DOI:10.1002/9783527829026

quantitative data from the TRMC results, including charge carrier mobilities and trap densities. The third section presents the TRMC measurements on $MAPbI_3$ and $MAPbBr_3$ including analysis of the decay kinetics. The found mobilities will be discussed and compared to other reported values determined by e.g. terahertz spectroscopy. In the last section TRMC measurements on both MHPs supplied with different CSTLs are presented. The CSTLs comprise Spiro-OMeTAD as a hole transport layer or C60 as electron transport layer. Possible implications of the mobilities and trap densities, which determine the charge carrier diffusion lengths, on the charge collection and performance of a corresponding cell will be discussed.

Section 1: Time-Resolved Microwave Conductivity

The TRMC technique can be used to study the dynamics of photo-induced charge carriers in semiconductor materials with low background conductivities.[6–10] This technique is based on the interaction between the electric field component of the microwaves (GHz regime) and mobile carriers (see Figure 1). Hence, the photoconductivity can be determined without contacting the semiconductor to electrodes, thereby avoiding interfacial effects or undesired chemical reactions between the MHP and the metallic electrodes.[11,12]

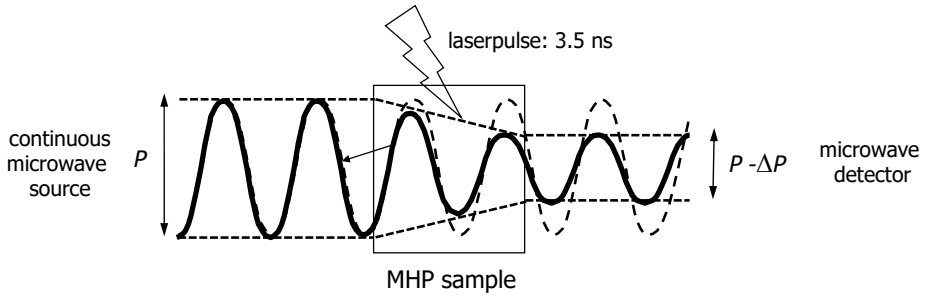

Figure 1. Representation of photo-induced time-resolved microwave conductivity technique. In essence the MHP is optically excited by a short laser pulse, yielding excess charge carriers. These carriers interact with microwaves, resulting in a reduction of the microwave power which is measured on nanosecond timescales. TRMC is used to measure the photo-conductance, which scales with the time-dependent concentration n and mobility μ of free electrons and holes.

Published in: Halide Perovskite Semiconductors: Structures, Characterization, Properties, and Phenomena - Editor(s):Yuanyuan Zhou, Iván Mora Seró - DOI:10.1002/9783527829026

The sinusoidal (dashed) line represents the magnitude of the microwave electric field as it passes through the (excited) MHP.

In general, if photo-excitation of a material results in the generation of free, mobile charge carriers, the conductivity of this material changes. The electrical conductivity, σ scales with the concentration of free charge carriers, n and their mobility μ according to:

$$\sigma = e \sum_i n_i \mu_i \quad (1)$$

where e is the elementary charge. With the TRMC technique, the integrated change in σ over the complete film thickness, L, is measured, which yields a change in conductance, ΔG:

$$\Delta G = \beta \int_0^L \Delta\sigma(z)\, dz \quad (2)$$

Here β is the ratio between the wide and small inner walls of the microwave guide. Hence, ΔG is proportional to the product of the total number of photo-induced free charges and their mobility. Absorption of microwaves by the free carriers reduces the microwave power on the detector. The normalized reduction in microwave power $(\Delta P(t))/P$ is related to $\Delta G(t)$ by:

$$\frac{\Delta P(t)}{P} = -K\Delta G(t) \quad (3)$$

where K is the sensitivity factor, which can be quantified as described previously.[10,13]

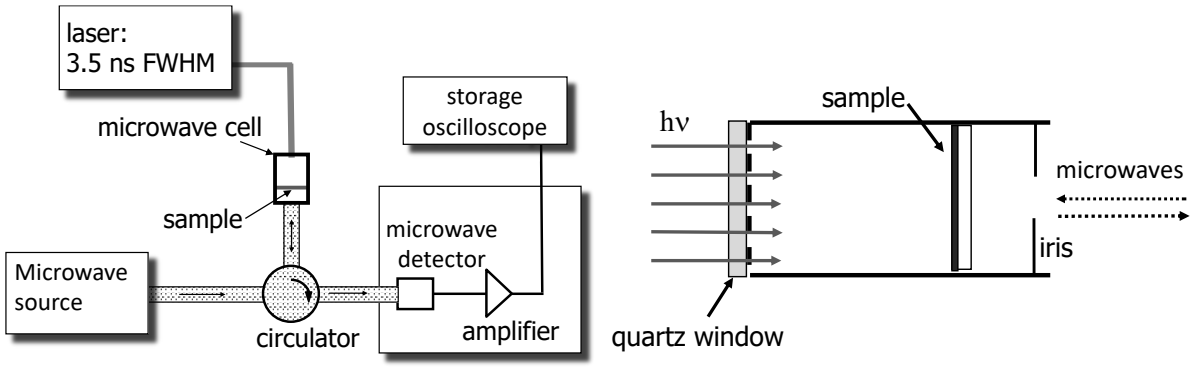

Figure 2. Schematic representation of (left) the TRMC set-up and (right) the TRMC cell. Adapted from Savenije et al.[8]

Published in: Halide Perovskite Semiconductors: Structures, Characterization, Properties, and Phenomena - Editor(s):Yuanyuan Zhou, Iván Mora Seró - DOI:10.1002/9783527829026

Figure 2 shows a representation of the TRMC set up. Photo-excitation is realized by laser pulses of 3-5 ns FWHM with a tunable wavelength at a repetition rate of 10 Hz. Metallic, neutral density filters with different optical densities are applied to vary the photon fluence between 10^9 and 10^{15} photons/cm^2 per pulse. A voltage-controlled oscillator is utilised to generate the microwaves with a frequency in the 10 GHz range. The sample of interest is placed in a microwave cell that ends with a metal grating (see Figure 2b), which largely transmits the laser power, but fully reflects the microwaves. A quartz window is glued on top of the grating to seal the cell and avoid air exposure of the sample. In the presence of an iris (see Figure 2b) the sensitivity factor, *K* is much higher (ca 40 times) than for an iris free microwave cell. However, this sensitivity gain leads to an increase of the response time from ca 1 ns to 18 ns. A microwave diode detector converts the microwave power into a transient voltage which is recorded using a digital oscilloscope.

If the sensitivity factor *K* is known, ΔG can be quantitatively obtained from the measured $\Delta P(t)/P$ using Eq. 3. Then, the TRMC signal can be expressed in the remaining two unknown parameters: *i.e.* the mobility, μ and the charge carrier generation yield, φ. If every absorbed photon creates a single positive and a negative charge carrier, Eq. 1 simplifies to:

$$\sigma = en(\mu_e + \mu_h) \quad (4)$$

in which *n* is the concentration, μ_e is the electron mobility and μ_h is the hole mobility. The yield can be defined as

$$\varphi = \frac{Ln}{F_A I_0} \quad (5)$$

in which I_0 is the intensity of the laser in photons/pulse/unit area and F_A is the fraction of light absorbed at the excitation wavelength. By combining Eqs. 2, 4 and 5, the product of yield and mobility can be obtained from ΔG_{max}

$$\varphi(\mu_e + \mu_h) = \frac{Ln}{F_A I_0}\frac{\Delta\sigma}{en} = \frac{L}{F_A I_0}\frac{\Delta G_{max}}{e\beta L} = \frac{\Delta G_{max}}{F_A I_0 e\beta} \quad (6)$$

Published in: Halide Perovskite Semiconductors: Structures, Characterization, Properties, and Phenomena - Editor(s):Yuanyuan Zhou, Iván Mora Seró - DOI:10.1002/9783527829026

Expressing the TRMC signal in $\varphi(\mu_e + \mu_h)$ product enables us to directly compare TRMC measurements of different samples.

In contrast to DC techniques, such as time-of-flight or field effect transistor measurements, charges do not undergo a net displacement in the photo-active layer during a TRMC measurement. In fact, due to the low electric field strength of the microwaves in the cell and the rapid oscillating direction of the electric field, the drift distances are relatively small, *i.e.* in the nanometer regime. This implies that transport over grain boundaries does not limit the mobilities unless the grain size becomes <100 nm.[14] For techniques in which excess carriers have to cross grain boundaries, reported mobilities are typically at least an order of magnitude less.[15] An extensive discussion over the latter is reported for thin films of $MAPbI_3$ by Levine et al.[16]

Note that both electrons and holes' contributions to the photo-conductance depend on their mobilities. This is in contrast with more frequently used time-resolved photoluminescence (TRPL) measurements, which specifically detects radiative recombination events. Therefore, the decays obtained with TRMC cannot a priori be compared to TRPL signals. Instead, TRMC gives complementary insights to TRPL, since it displays the recombination of all free mobile charge carriers: both radiative and non-radiative. Therefore, TRMC is especially useful for studying the recombination kinetics in MHPs showing poor light-outcoupling and substantial reabsorption of emitted photons, such as macroscopic MHP crystals, or MHPs supplied with a transport material, where most recombination is non-radiative.

Section 2: Global modelling of TRMC Data

In order to extract quantitative data out of TRMC measurements, the generic kinetic model, as detailed in Figure 3 can be used.[17,18] This model accounts for different recombination pathways of photo-excited electrons and holes and assumes homogeneous generation and decay of

Published in: Halide Perovskite Semiconductors: Structures, Characterization, Properties, and Phenomena - Editor(s):Yuanyuan Zhou, Iván Mora Seró - DOI:10.1002/9783527829026

charges, which can be experimentally realized by using an excitation wavelength close to the absorption onset. In view of the relatively small exciton binding energy of most MHPs compared to thermal energy,[19] electron-hole pairs dissociate into free CB electrons and VB holes.

Formation of charge carriers is represented by the generation term, G_C and takes into account the temporal profile and total light intensity of the laser pulse. In general, perovskite semiconductors are often unintentionally doped due to impurities and defects states in the crystal lattice. This leads to additional CB electrons (n-type) or VB holes (p-type) already present before photo-excitation. In case of a p-type doped perovskite as shown in Figure 3, the concentration of dark carriers is represented by p_0. Note that p_0 does not contribute to the photo-conductance since the TRMC technique is an AC technique, however p_0 affects the recombination rates.

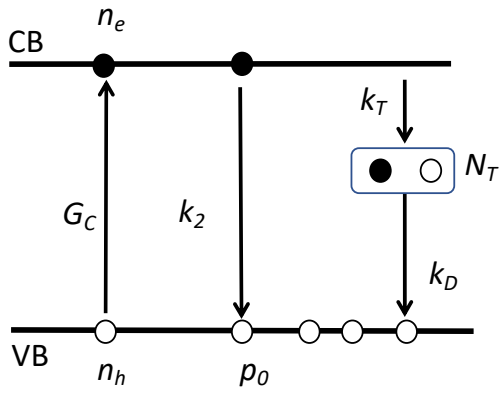

Figure 3. Kinetic model of processes occurring upon photo-excitation of a (unintentionally) p-type semiconductor perovskite. Here, G_C represents the photo-excitation of electrons (closed circles) from the valence band (VB) to the conduction band (CB). The CB electrons can recombine with holes (open circles) in the VB via k_2. In competition with k_2, electrons can be immobilized in intra-band gap trap states with total density N_T via k_T. Finally, the trapped electrons can recombine with holes from the VB via k_D. In the case of an (unintentionally)

Published in: Halide Perovskite Semiconductors: Structures, Characterization, Properties, and Phenomena - Editor(s):Yuanyuan Zhou, Iván Mora Seró - DOI:10.1002/9783527829026

doped MHP, there will be additional holes (p_0, p-type) on top of the photo-generated holes. Note that this fully mathematical model also holds for an n-type MHP with trap states for holes. The following set of coupled differential equations implements the processes shown in Figure 3 and describes n_e (Eq. 7) n_h (Eq. 8) and n_t (Eq. 9) as function of time. The rate constants for band-to-band electron-hole recombination, trap filling and trap emptying are represented by k_2, k_T and k_D respectively.

$$\frac{dn_e}{dt} = G_c - k_2 n_e(n_h + p_0) - k_T n_e(N_T - n_t) \quad (7)$$

$$\frac{dn_h}{dt} = G_c - k_2 n_e(n_h + p_0) - k_D n_t(n_h + p_0) \quad (8)$$

$$\frac{dn_t}{dt} = k_T n_e(N_T - n_t) - k_D n_t(n_h + p_0) \quad (9)$$

Solving the equations using numerical methods yields the time-dependent concentrations n_e, n_h and n_t. The change in photo-conductance as function of time is calculated from the product of charge carrier concentrations and mobilities according to:

$$\Delta G(t) = e(n_e(t)\mu_e + n_h(t)\mu_h)\beta L \quad (10)$$

Here, the trapped charge carriers, n_t are assumed to be immobile and do not contribute to ΔG. The mobilities are assumed to be constant within the time window of the measurement and independent of the charge density. Finally, a convolution is applied to take into account the instrumental response function of the set-up.[10] To obtain accurate values for all kinetic parameters describing a specific MHP, a set of TRMC traces induced by widely varying laser intensities (preferably more than two orders of magnitude) should be recorded. Fits to these TRMC traces vary only by adapting the laser intensity, which is incorporated in the generation term, G_C. By following this global approach accurate quantification of all parameters is feasible.

Published in: Halide Perovskite Semiconductors: Structures, Characterization, Properties, and Phenomena - Editor(s):Yuanyuan Zhou, Iván Mora Seró - DOI:10.1002/9783527829026

Section 3. TRMC measurements on $MAPbI_3$ and $MAPbBr_3$

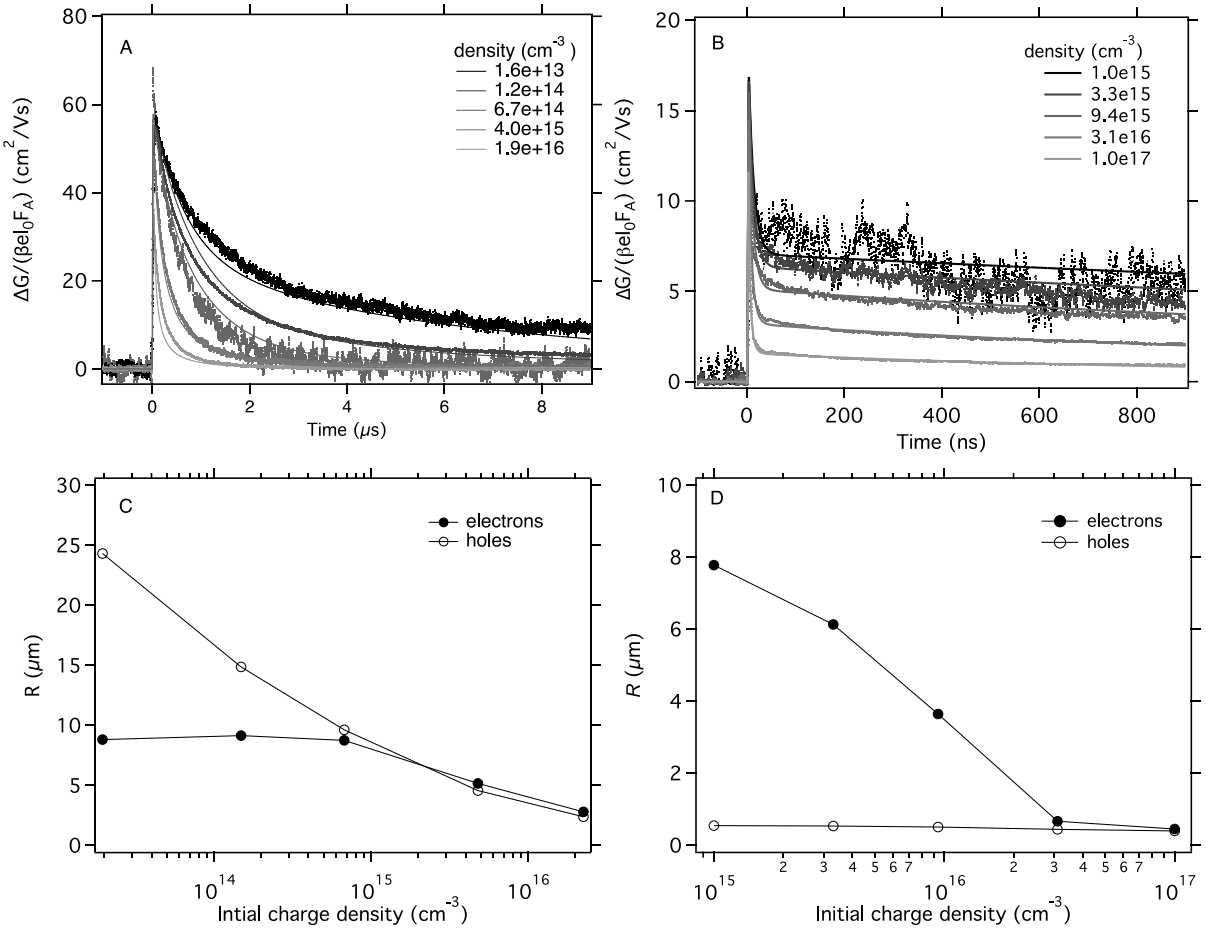

Figure 4. Experimental TRMC traces for (a) $MAPbI_3$ and (b) $MAPbBr_3$ recorded at wavelengths of λ = 650 nm and 500 nm, respectively. The full lines are calculated by numerically solving differential equations (7-9) and converting the time-dependent concentration curves to the light intensity normalized ΔG traces. Note the difference in time scale! Panels (c) and (d) show the calculated charge carrier diffusion lengths on basis of charge carrier lifetime ($t_{1/2}$) and mobility for different laser intensities. Adapted from Zhao et al.[29]

Results from TRMC measurements on MHPs are provided in Figures 4a and 4b for $MAPbI_3$ and $MAPbBr_3$, respectively. The photo conductance, normalized for the number of absorbed photons is shown as function of time on photo-excitation using incident light intensities ranging

Published in: Halide Perovskite Semiconductors: Structures, Characterization, Properties, and Phenomena - Editor(s):Yuanyuan Zhou, Iván Mora Seró - DOI:10.1002/9783527829026

over at least two orders of magnitude. The rise of the signal at t = 0 originates from the formation of mobile excess charges; the maximum signal height reflects the product of charge carrier generation yield and the mobility. For $MAPbI_3$ at higher intensities, the decay kinetics become increasingly faster, which is typically observed in a regime where higher order recombination dominates. Apart from this also the maximum signal somewhat reduces due to the fact that in pulse recombination occurs. At very low excitation densities the number of generated excess carriers is below the trap density. For these excitation intensities the band to band second order recombination process is not the dominant decay process any more due to the rapid trapping of the minority carriers. Note that at this intensities, the counter charges are responsible for the observed TRMC signal as these are still mobile. Most notably for $MAPbBr_3$ we observe very different decay kinetics, featuring a very fast, sharp decrease followed by a long-lived almost constant signal. In analogy with $MAPbI_3$ at higher intensities the normalised TRMC becomes increasingly smaller.

Using the kinetic model as described in Section 2, the TRMC traces for both MHPs are fitted using a single set of kinetic parameters and results are collected in Table 1. Note that for obtaining the different TRMC traces, only the magnitude of the generation term, G_c is altered according to the incident intensity. Despite the very different decay kinetics for both MHPs we see that the model describes the TRMC traces for both MHPs rather well. Using this approach it is feasible to obtain accurate values for all kinetic parameters describing the charge carrier dynamics. Some prominent dissimilarities between both MHPs can be observed including mobilities, band-to-band recombination rate constants, and values for the trap - and back-ground density. For $MAPbI_3$ layers mobilities between 50 and 100 cm^2/Vs are close to previously reported values measured using TRMC or optically pump terahertz probe measurements (OPTP).[16,20,21] From Table 1 there is a clear difference between the mobilities of $MAPbI_3$ and $MAPbBr_3$. The mobility according to the classical Drude model is given by

Published in: Halide Perovskite Semiconductors: Structures, Characterization, Properties, and Phenomena - Editor(s):Yuanyuan Zhou, Iván Mora Seró - DOI:10.1002/9783527829026

$$\mu = \frac{e\tau}{m^*} \quad (11)$$

in which τ is the scattering time and m^* the effective mass. From first principles calculations or magneto-optical studies the effective masses of the charge carriers have been derived, which show similar values for electrons and holes of $0.10m_0$ to $0.2m_0$ for both materials.[22–24] With respect to the scattering time, τ it has been argued that the interactions between the longitudinal phonon modes are higher for bromide perovskites than iodide perovskites. The resulting shorter scattering times for $MAPbBr_3$ provides an explanation for the differences in the observed mobilities.[25] The values for k_2 for $MAPbI_3$ are very close to previously reported numbers.[26] The higher value for k_2 for $MAPbBr_3$ might find its origin in surface enhanced second order recombination as recently deduced.[29]

Table 1. Kinetic parameters used for fits to the TRMC traces for bare $MAPbI_3$ and $MAPbBr_3$ layers.

	$MAPbI_3$	$MAPbBr_3$
k_2 [x 10^{-9} cm^3 s^{-1}]	1.2	5.5
k_T [x 10^{-9} cm^3 s^{-1}]	8	2
k_D [x 10^{-10} cm^3 s^{-1}]	0.5	0.45
N_T [x 10^{15} cm^{-3}]	0.2	35
p_0 / n_0 [x 10^{15} cm^{-3}]	0.02	3.5
μ_e [cm^2 $(Vs)^{-1}$]	75	9.5
μ_e [cm^2 $(Vs)^{-1}$]	50	9.5

Next, we discuss the large difference in trap densities found in $MAPbI_3$ and $MAPbBr_3$. The density of the latter is more than 2 orders of magnitude larger. Same is true for the number of dark carriers. The number of traps has of course major effects on the charge dynamics, which is evident from the TRMC decay kinetics shown in Figures 4a and 4b. From the parameters we can calculate the lifetime of a carrier in the conduction or valence band. Knowing the half lifetime, $\tau_{1/2}$ and the mobilities enables us to get an idea about the charge carrier diffusion length, R using:

Published in: Halide Perovskite Semiconductors: Structures, Characterization, Properties, and Phenomena - Editor(s):Yuanyuan Zhou, Iván Mora Seró - DOI:10.1002/9783527829026

$$R = \sqrt{D\tau_{\frac{1}{2}}} \quad (12)$$

The diffusion coefficient, D can be derived from the charge mobility obtained by fitting of the TRMC traces and using the Einstein-Smoluchowski equation, $D = kT\mu/e$. As shown in Figure 4c, R for the minority carriers in $MAPbI_3$ is very small in comparison to that of the majority carriers. At excitation intensities yielding a charge carrier concentration just below N_T we observe that the values of R for both electrons and holes are similar and maximal. At higher densities R becomes smaller for both types of carriers due to enhanced band-to-band recombination. Thus, the electron and hole diffusion lengths are most balanced at charge densities just above the trap density, which is desirable for optimum collection of both electrons and holes in an operating solar cell.

In Figure 4d the R values are provided for $MAPbBr_3$. In particular for the minority carriers we see very short values, which can be explained by the fact that minority carriers get trapped on very short time scales. Only at very high laser intensities both diffusion lengths become similar. However, at these laser intensities also rapid band-to-band recombination is operative due to the corresponding high concentrations. Hence, generally substantially shorter values of R are found for $MAPbBr_3$. In summary we conclude that due to smaller mobility values as well as the substantially larger concentration of deep trap states, the charge carrier diffusion lengths in particular for the minority carriers in $MAPbBr_3$, are much smaller than those in $MAPbI_3$.

4. TRMC measurements on $MAPbI_3$ and $MAPbBr_3$ with charge selective contacts

Published in: Halide Perovskite Semiconductors: Structures, Characterization, Properties, and Phenomena - Editor(s):Yuanyuan Zhou, Iván Mora Seró - DOI:10.1002/9783527829026

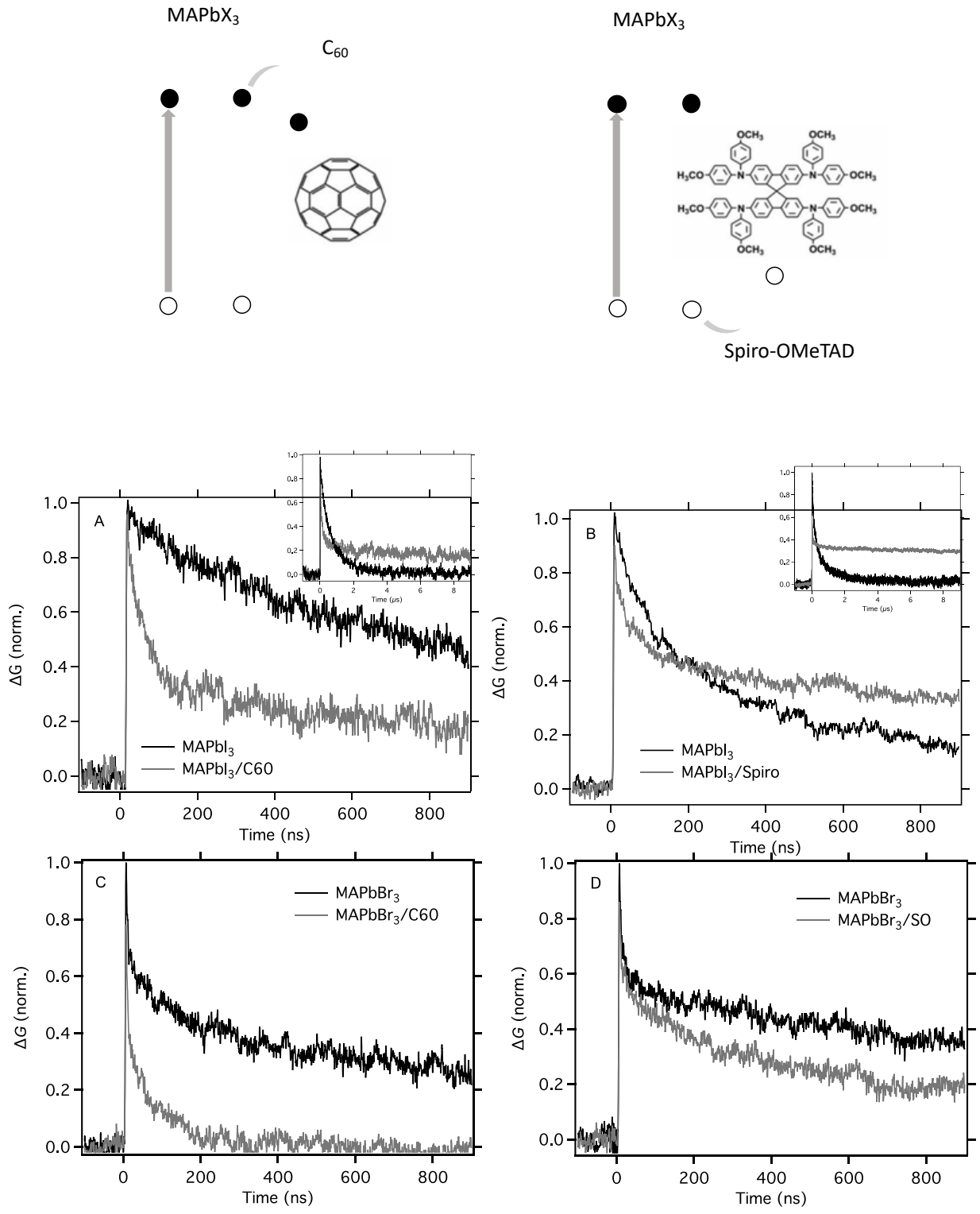

Figure 5. Top panels illustrate the charge extraction process: For left panels the CSTL is C60 while for the right panels the CSTL is Spiro-OMeTAD. A and B show the TRMC traces recorded at initial charge carrier densities of 5 - 10 x 10^{14} cm^{-3}/pulse for single and double layers comprising $MAPbI_3$ with excitation at λ = 650. C and D are the traces for $MAPbBr_3$ with

Published in: Halide Perovskite Semiconductors: Structures, Characterization, Properties, and Phenomena - Editor(s):Yuanyuan Zhou, Iván Mora Seró - DOI:10.1002/9783527829026

excitation at λ = 500 nm. The signal of the bare MHP layer is normalised to 1, while the bilayer is normalised with the same factor. Insets show TRMC traces on 10 microsecond timescale. Adapted from Zhao et al.[29]

While in the previous part we focused on mobilities and trap states, in this part we want to elucidate the type of carriers and traps responsible for the observed charge carrier dynamics. Since TRMC does not differentiate between holes and electrons and both carriers contribute to the photo conductance according to equation 1, other specific methods need to be invoked. To reveal which type of carrier is the minority carrier for both layers, we deposited on top of the MHP a CSTL. As electron accepting layer we used C60 while for hole transport layer Spiro-OMeTAD was used (See diagrams at top of Figure 5). Figure 5 shows the effect of introducing the CSTL on $MAPbI_3$ and $MAPbBr_3$, together with the bare MHP using identical laser wavelengths and intensities. The signal of the bare MHP layer is normalised to 1, and the bilayer is normalised with the same factor. As discussed previously, two important aspects can be noticed;[27–29] First the signal for all bilayers drops quickly below the signal of the bare perovskite layer. Obviously the CSTLs efficiently extract part of the carriers. Since the mobilities for electrons in C60 and for holes in spiro-OMeTAD are both smaller than in the perovskite, the overall TRMC signal lowers. Thus, it is important to realise that the predominant part of the TRMC signal is due to counter charges remaining in the perovskite. Interestingly for $MAPbI_3$ based bilayers both insets show that the charge carrier lifetimes extend over many microseconds, implying that recombination of the extracted carrier by the CSTL with the remaining counter charge is rather slow. If full extraction of either electrons or holes to a CSTL would occur, it is feasible to asses the mobility of the counter charge. However, since apart from charge extraction also charge trapping and band-to-band recombination occurs simultaneously, extraction is most likely not complete. However we do see that similar long-

lived signals appear for both CSTLs indicating that extraction for both transport layers takes place and that the charge carrier mobilities are close to balanced.[30] In conclusion we can state that for $MAPbI_3$ both charge carriers are both extracted efficiently and that charge carrier mobilities are comparable. The latter is in line with the results from the fits to the bare layers. Finally, we observe a very different behaviour for the bilayers with $MAPbBr_3$. For $MAPbBr_3$/C60 the signal drops down quickly to almost zero, while for the $MAPbBr_3$/spiro-OMeTAD the differences with the bare layer are limited. Combining this information with the results from the fits from Section 3, which revealed large amounts of deep trap states, we can conclude that these states form traps for holes and the majority mobile carriers are electrons. This can be rationalized as follows: Optical excitation of $MAPbBr_3$ leads to generation of excess carriers of which the holes are quickly trapped. These trapped holes are not able to get extracted by the Spiro-OMeTAD, while the C60 rapidly extracts the electrons. In the latter bilayer we conclude that no highly mobile carriers remain, since the mobility in C60 is <1 cm^2/Vs and the corresponding holes are rapidly trapped in $MAPbBr_3$, explaining the fast decaying signal. These observations can explain the typically poor performances observed for solar cells based on $MAPbBr_3$. Hence by combining the perovskite layer with transport layers specific information can be obtained regarding the type of minority carriers and of deep traps.

In the first two sections of this chapter we presented the basics of the time-resolved microwave technique and the analysis of decay kinetics. TRMC is a contactless technique and thus, it does not require prolonged exposure to electric fields that can potentially lead to ion migration in perovskites making it a very attractive method to study charge dynamics.[31] Additionally, photogeneration can occur over a broad range of intensities in the 1-sun equivalent regime.[16] In section 3 and 4 we applied this technique to $MAPbI_3$ and $MAPbBr_3$ with and without CSTLs. Analysis of the fits on the bare layers recorded using various light intensities yields the kinetic

Published in: Halide Perovskite Semiconductors: Structures, Characterization, Properties, and Phenomena - Editor(s):Yuanyuan Zhou, Iván Mora Seró - DOI:10.1002/9783527829026

parameters describing the charge carrier dynamics. From the bilayers, specific information regarding the electron and hole mobility can be obtained as well as the sign of the carriers. While $MAPbI_3$ can be regarded as highly intrinsic with doping densities $p_0 < 10^{14}$ cm^{-3}, $MAPbBr_3$ behaves as unintentional n-type doped with $n_0 > x\ 10^{15}$ cm^{-3}. Furthermore, the high number of deep trap states makes the charge carrier diffusion length of the minority carriers in $MAPbBr_3$ small, < 0.5 μm, which is typically not sufficient for optimal solar cell performance. In this chapter we have shown that the TRMC technique is able to reveal the charge carrier dynamics on timescales relevant for opto-electronic devices. The versatile and electrodeless nature of the technique allows screening of perovskite layers with differences in material composition or deposition method.

Supporting Information
Supporting Information is available from the Wiley Online Library or from the author.

Acknowledgements

This work was supported by the Netherlands Organization for Scientific Research (NWO) under the Echo grant number: 712.014.007.

References

[1] A. Kojima, K. Teshima, Y. Shirai, T. Miyasaka, *J. Am. Chem. Soc.* **2009**, *131*, 6050.
[2] J. H. Im, C. R. Lee, J. W. Lee, S. W. Park, N. G. Park, *Nanoscale* **2011**, *3*, 4088.
[3] M. J. P. Alcocer, T. Leijtens, L. M. Herz, A. Petrozza, H. J. Snaith, *Science (80-.).* **2013**, *342*, 341.
[4] W. S. Yang, B. W. Park, E. H. Jung, N. J. Jeon, Y. C. Kim, D. U. Lee, S. S. Shin, J. Seo, E. K. Kim, J. H. Noh, S. Il Seok, *Science (80-.).* **2017**, *356*, 1376.
[5] NREL, *Best Res. Effic. Chart, Photovolt. Res.* **2022**, https://www.nrel.gov/pv/cell.
[6] J. E. Kroeze, T. J. Savenije, M. J. W. Vermeulen, J. M. Warman, *J. Phys. Chem. B* **2003**, *107*, 7696.
[7] J. M. Warman, M. P. De Haas, G. Dicker, F. C. Grozema, J. Piris, M. G. Debije, *Chem. Mater.* **2004**, *16*, 4600.

[8] T. J. Savenije, A. J. Ferguson, N. Kopidakis, G. Rumbles, *J. Phys. Chem. C* **2013**, *117*, 24085.
[9] H. Oga, A. Saeki, Y. Ogomi, S. Hayase, S. Seki, *J. Am. Chem. Soc.* **2014**, *136*, 13818.
[10] E. M. Hutter, T. J. Savenije, C. S. Ponseca Jr, in *Perovskite Sol. Cells Princ. Mater. Devices*, World Scientific Publishing Co. Pte. Ltd., **2017**, pp. 179–232.
[11] R. A. Kerner, P. Schulz, J. A. Christians, S. P. Dunfield, B. Dou, L. Zhao, G. Teeter, J. J. Berry, B. P. Rand, *APL Mater.* **2019**, *7*, DOI 10.1063/1.5083812.
[12] L. Zhao, R. A. Kerner, Z. Xiao, Y. L. Lin, K. M. Lee, J. Schwartz, B. P. Rand, *ACS Energy Lett.* **2016**, *1*, 595.
[13] O. G. Reid, D. T. Moore, Z. Li, D. Zhao, Y. Yan, K. Zhu, G. Rumbles, *J. Phys. D. Appl. Phys.* **2017**, *50*, DOI 10.1088/1361-6463/aa9559.
[14] L. A. Muscarella, E. M. Hutter, S. Sanchez, C. D. Dieleman, T. J. Savenije, A. Hagfeldt, M. Saliba, B. Ehrler, *J. Phys. Chem. Lett.* **2019**, *10*, 6010.
[15] K. S. Haber, A. C. Albrecht, *J. Phys. Chem.* **1984**, *88*, 6025.
[16] I. Levine, S. Gupta, A. Bera, D. Ceratti, G. Hodes, D. Cahen, D. Guo, T. J. Savenije, J. Ávila, H. J. Bolink, O. Millo, D. Azulay, I. Balberg, *J. Appl. Phys.* **2018**, *124*, DOI 10.1063/1.5037637.
[17] S. D. Stranks, V. M. Burlakov, T. Leijtens, J. M. Ball, A. Goriely, H. J. Snaith, *Phys. Rev. Appl.* **2014**, *2*, 1.
[18] E. M. Hutter, G. E. Eperon, S. D. Stranks, T. J. Savenije, *J. Phys. Chem. Lett.* **2015**, *6*, 3082.
[19] A. Miyata, A. Mitioglu, P. Plochocka, O. Portugall, J. T. W. Wang, S. D. Stranks, H. J. Snaith, R. J. Nicholas, *Nat. Phys.* **2015**, *11*, 582.
[20] R. Brenes, D. Guo, A. Osherov, N. K. Noel, C. Eames, E. M. Hutter, S. K. Pathak, F. Niroui, R. H. Friend, M. S. Islam, H. J. Snaith, V. Bulović, T. J. Savenije, S. D. Stranks, *Joule* **2017**, *1*, 155.
[21] L. M. Herz, *ACS Energy Lett.* **2017**, *2*, 1539.
[22] F. Brivio, K. T. Butler, A. Walsh, M. Van Schilfgaarde, *Phys. Rev. B - Condens. Matter Mater. Phys.* **2014**, *89*, 1.
[23] K. Galkowski, A. Mitioglu, A. Miyata, P. Plochocka, O. Portugall, G. E. Eperon, J. T. W. Wang, T. Stergiopoulos, S. D. Stranks, H. J. Snaith, R. J. Nicholas, *Energy Environ. Sci.* **2016**, *9*, 962.
[24] L. D. Whalley, J. M. Frost, Y. K. Jung, A. Walsh, *J. Chem. Phys.* **2017**, *146*, DOI 10.1063/1.4984964.
[25] A. D. Wright, C. Verdi, R. L. Milot, G. E. Eperon, M. A. Pérez-Osorio, H. J. Snaith, F. Giustino, M. B. Johnston, L. M. Herz, *Nat. Commun.* **2016**, *7*, DOI 10.1038/ncomms11755.
[26] C. L. Davies, M. R. Filip, J. B. Patel, T. W. Crothers, C. Verdi, A. D. Wright, R. L. Milot, F. Giustino, M. B. Johnston, L. M. Herz, *Nat. Commun.* **2018**, *9*, 1.
[27] E. M. Hutter, J. J. Hofman, M. L. Petrus, M. Moes, R. D. Abellón, P. Docampo, T. J. Savenije, *Adv. Energy Mater.* **2017**, *7*, DOI 10.1002/aenm.201602349.
[28] V. M. Caselli, Z. Wei, M. M. Ackermans, E. M. Hutter, B. Ehrler, T. J. Savenije, *ACS Energy Lett.* **2020**, *5*, 3821.
[29] J. Zhao, V. M. Caselli, M. Bus, B. Boshuizen, T. J. Savenije, *ACS Appl. Mater. Interfaces* **2021**, *13*, 16309.
[30] C. S. Ponseca, T. J. Savenije, M. Abdellah, K. Zheng, A. Yartsev, T. Pascher, T. Harlang, P. Chabera, T. Pullerits, A. Stepanov, J. P. Wolf, V. Sundström, *J. Am. Chem. Soc.* **2014**, *136*, 5189.
[31] M. H. Futscher, J. M. Lee, L. McGovern, L. A. Muscarella, T. Wang, M. I. Haider, A. Fakharuddin, L. Schmidt-Mende, B. Ehrler, *Mater. Horizons* **2019**, *6*, 1497.

Published in: Halide Perovskite Semiconductors: Structures, Characterization, Properties, and Phenomena - Editor(s):Yuanyuan Zhou, Iván Mora Seró - DOI:10.1002/9783527829026